Underwater and Surface Obstacle Detection with Stereo Vision Method for USV Collision Avoidance Risk Assessment in Shallow Water

Kaiwen Xue[1], Jiawei Liu[2], Nan Xiao[2], Xiaoqiang Ji[1] and Huihuan Qian[1,‡]

***Abstract*— This paper originally proposes a method to combine underwater and surface obstacle detection for collision avoidance of a USV exploring an unknown environment in the field. In our method, the surface and underwater obstacles are detected simultaneously with only one stereo camera and an IMU. Then, the underwater obstacles measurement inaccuracy caused by the refraction at the water-air boundary is photogrammetrically corrected by the proposed depth correction model. Furthermore, the wave-induced motion of the USV is modeled using the time-frequency analysis to estimate a safe exploration area. Both the indoor and outdoor experiments have verified the proposed method, which quantitatively achieves a 65.44% improvement of the depth compared with the direct measurement from the air on average in the sample sets of our experiments. The proposed method can significantly improve the safety and expand the working area for the USV during the exploration in shallow water. It provides an option for collision avoidance in clear and shallow waters.**

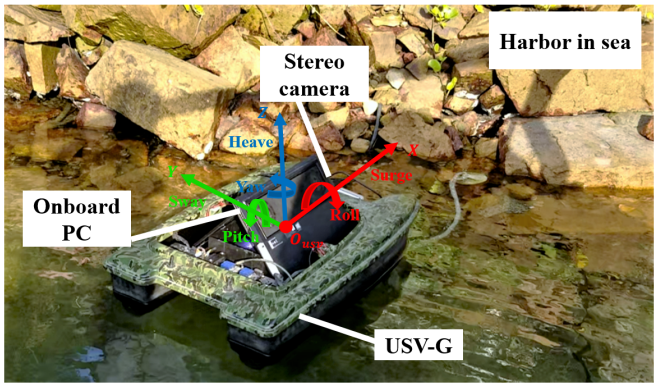

Fig. 1. A USV is exploring a harbor nearshore in sea with a stereo camera and an onboard PC. The water waves will induce the USV motions along the XYZ axis and result in roll, yaw, pitch and surge, sway, heave accordingly.

I. INTRODUCTION

Unmanned Surface Vehicles (USVs) have become the main platform for various tasks in water environment [1], ranging from commercial, scientific to transportation demands [15], etc. Thanks to the compact dimensions of USVs and the great maneuverability, they are capable of performing challenging tasks in more hazardous and cluttered environments, and thus provide an ideal platform for tasks in an unknown environment on water. Field exploration of caves and shallow rivers in primitive rain forests [13], water-borne microorganism sampling [16], nearshore plants specimen sampling with the USV, for all these complex tasks in shallow water, both the surface and underwater obstacles present significant threats to the USVs operations.

There exist various methods of surface obstacles detection for USVs. The dominant sensors include Lidar [5], stereo or monocular cameras [4][3], radar [7] and the fusion of sensors [13][6]. For underwater obstacle detection and avoidance, the most popular sensor is sonar [2][8][9][12] and cameras [10][11] for both underwater robots and USVs. However, the sonar measurement range varies from decimeters [14] to hundred meters [9][12]. For small-sized USVs of 1 to 3 meters with weight less than 1 ton, their drafts are typically less than within centimeters. Besides, their cost are typically high and the underneath installation may face threats by underwater obstacles. Therefore, for these small-sized USVs in shallow water, cameras tend to be a more promising sensor for underwater obstacle detection for their installation position and low cost. Besides, the continuous water disturbance will cause significant heaving and result in collision with the underwater obstacles. Generally, the path planning methods for USVs can only guarantee a plausible path without obstacles [9]. For exploration in shallow water, the goal is to explore as much area as possible while keeping the USV safe from the underwater obstacles. In this situation, we propose a safety-assurance risk assessment considering the water disturbance and the underwater obstacles.

In this paper, we firstly propose a method aiming to fill the gap of underwater and surface obstacle detection with only one stereo camera simultaneously for the USVs community. A depth correction model is proposed to tackle the raw measurement error of the underwater obstacle depth caused by light refraction. Besides, the wave-induced heave motion of the USV in water disturbance is analyzed and incorporated to provide the USVs with a safety strategy during exploration. This method will enable the USVs with more capabilities to perform exploration tasks in shallow water.

The rest of this paper is organized as follows: the overall system of the proposed obstacle detection method is presented in Section II. Section III stresses the depth correction model for the underwater obstacles, and Section IV focuses on the wave-induced motion modeling and risk assessment. Section V details field experiments results and analysis. Finally, Section VI concludes the paper.

II. SYSTEM OVERVIEW

As shown in Fig.2, our system mainly consists of two parts: underwater obstacle depth correction using the stereo

[1]Shenzhen Institute of Artificial Intelligence and Robotics for Society, The Chinese University of Hong Kong, Shenzhen.
[2]The Chinese University of Hong Kong, Shenzhen.
[‡]Corresponding author is Huihuan Qian, email: hhqian@cuhk.edu.cn

camera visual information and wave-induced motion modeling with the onboard IMU sample data. Our system aims at underwater and surface obstacles detection simultaneously, removing the depth distortion by light refraction and assuring the safety of the USVs during its exploration tasks in shallow water.

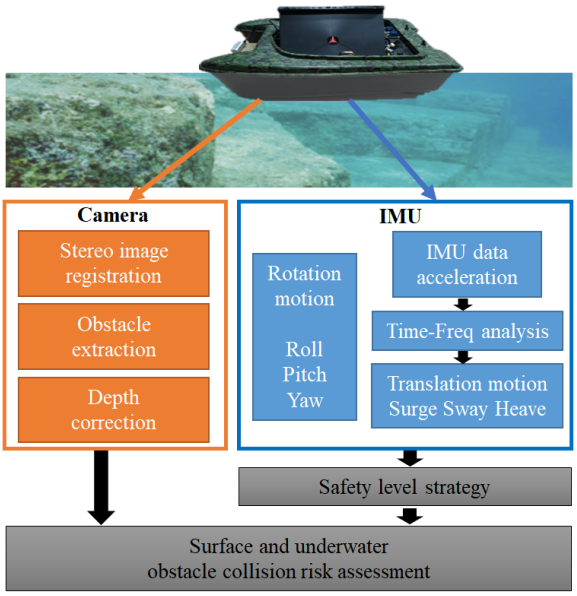

Fig. 2. System architecture of the proposed obstacle detection system.

A. Underwater Obstacle Depth Measurement Correction

This subsection mainly aims at processing and correcting the measured depth from the onboard stereo image sensor. As said in [19][20], the water-air boundary will induce the light refraction and result in a distortion of the true depth of the obstacles. In this section, images from the stereo camera will be used for image registration, and then the obstacles will be extracted based on the depth information. Furthermore, the light refraction error of the obstacles will be modeled and corrected. The rectified depth information of underwater obstacles will be used for obstacle detection and safety criteria for USVs.

B. Wave-induced USV Motion Modeling

In this part, we mainly focus on the wave-induced motion of the USVs with onboard IMU data. The wave will induce both translational and rotational movement of the USVs, and the onboard IMU will measure the motion information.

A time-frequency analysis of the IMU data will be performed to obtain the translational motion. The USV rotation angle will influence the incidence angle at the water-air boundary and the USV draft change. This will be addressed in the Section.IV-B. With the USV motion range and the draft of USVs, and the rectified underwater obstacles depth, collision avoidance risk assessment is proposed by defining different safety levels in water disturbance. The risk assessment will contribute to the USVs operation considering the surface and underwater obstacle detection.

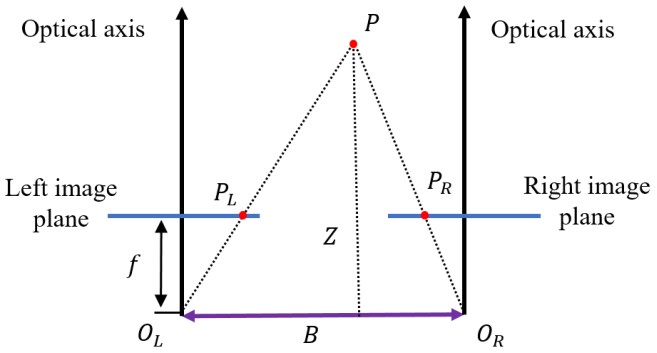

Fig. 3. Stereo images registration and depth extraction.

III. The Underwater Obstacle Measurement Correction Algorithm

In this section, the measured distorted depth of the underwater obstacles will be addressed. The proposed depth correction method can adjust the measured obstacle depth, and the rectified depth can be further used for the collision avoidance risk assessment. This can further provide valuable information for path planning and the safety strategy for the USVs operation in shallow water.

A. Stereo Image Matching

As shown in Fig.3, the left and right cameras sample the point P in the 3D world. With the baseline B and the focal length f known, and feature extraction of each pixel in the image, the disparity $P_L - P_R$ in pixels can be calculated. Then the depth information Z of each pixel can be obtained based on the similar triangles $\triangle PO_LO_R$ and $\triangle PP_LP_R$. Finally, the depth map from the left and right image plane of the stereo camera is obtained:

$$Z = \frac{Bf}{P_L - P_R} \tag{1}$$

In our system, an intel camera sensor Realsense D435i is used for retrieving the depth information of the environment. This camera implements a projector with structural light and two infrared cameras to extract the depth information.

B. Depth Correction Modeling With Snell's Law

As said above, the water-air boundary will induce light refraction, and thus the stereo camera will obtain distorted depth data. In this part, the refraction-induced error will be addressed and corrected. First, the light refraction at the water-air boundary will be modeled [19][20] as below:

As shown in Fig.4, the light rays SO_bO_c from the underwater objects S will suffer from the refraction at the boundary of the air and water. Therefore, the stereo camera will measure its depth information as the underwater object is in position S'. To model the geometry of the light rays refraction and the depth information, we define the coordinates as follows: O_w the origin of the world coordinate, O_c the origin of the camera with height h from the water surface, O_b the incidence position at the boundary, θ the incident angle, ϕ the refraction angle, γ the refractive index,

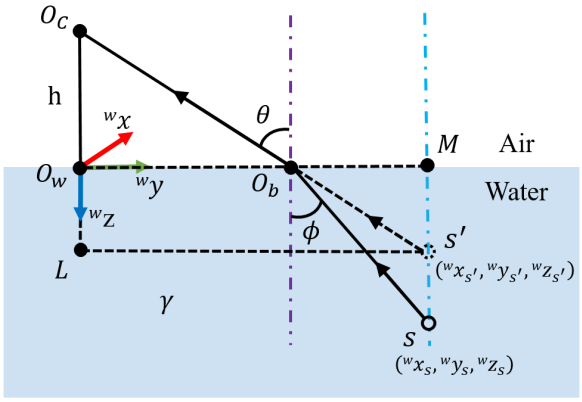

Fig. 4. Illustration of light refraction at the air-water boundary.

and L, M the intersection points with the extended lines. First, the measured position of the underwater object S from the stereo camera is the position of S' due to the refraction effect, and the world coordinate from the raw measured depth map can be easily retrieved as $({}^w x_{s'}, {}^w y_{s'}, {}^w z_{s'})$. To get the underwater object's correct depth information S, the geometry relations are further analyzed.

In $\triangle O_c L S'$, with $({}^w x_{s'}, {}^w y_{s'}, {}^w z_{s'})$ known, the following geometry holds:

$$\tan(\theta) = \frac{\sqrt{({}^w x_{s'})^2 + ({}^w y_{s'})^2}}{h + {}^w z_{s'}} \tag{2}$$

Then with the water refractive index γ=1.33 known, and based on Snell's law,

$$\gamma = \frac{\sin(\theta)}{\sin(\phi)} \tag{3}$$

After that, in $\triangle O_b S' M$, the length $l_{O_b M}$ of $O_b M$ is:

$$l_{O_b M} = \tan(\theta) * l_{MS'} = \tan(\theta) * {}^w z_{s'} \tag{4}$$

Finally, with $l_{O_b M}$ known, the rectified real depth ${}^w z_s$ of the underwater object S can be obtained in $\triangle O_b M S$ as

$${}^w z_s = \frac{l_{O_b M}}{\tan\phi} = \frac{{}^w z_{s'} \sqrt{({}^w x_{s'})^2 + ({}^w y_{s'})^2}}{\tan\phi (h + {}^w z_{s'})} \tag{5}$$

With all of the above, the raw depth information of underwater obstacles will be corrected, and this rectified depth information will guide the safety strategies for USVs exploration tasks in the field.

C. Discussions of The Light Refraction And Water Turbidity

The threats for the stereo cameras and our proposed depth correction modeling mainly come from the light refraction and water turbidity.

First, the light refraction on water is changing at any time, and it will propose challenges for the stereo image matching and depth extraction algorithm. Especially for the field experiments in a sea harbor, the strong light reflection causes many invalid pixels on the depth image from the realsense. In this situation, for simplicity and effectiveness, our proposed methods only perform on the valid pixels on the depth image discarding invalid pixels on the depth image.

As for the water turbidity requirement, it surely limits the proposed methods generality to some degree in terms of turbid water, but there exists limpid and clean waters in a lot of rivers, lakes and harbors nearshore. Our method is reasonably applicable for these waters during exploration tasks.

IV. Modeling of Wave-induced Motion of USVs

In this section, we mainly analyze the wave-induced USVs motion: translation (surge, sway, heave) and rotation (roll, pitch, yaw) as shown in Fig.1. The wave-induced translational motion of the USVs is measured by the onboard IMU. The IMU data is analyzed in the time-frequency domain and processed in real-time to represent the surge, sway and heave information as shown in Fig.5. This analysis will provide a guideline for designing the collision avoidance risk assessment for exploration tasks during the USVs operation in the field as shown in Algorithm.1.

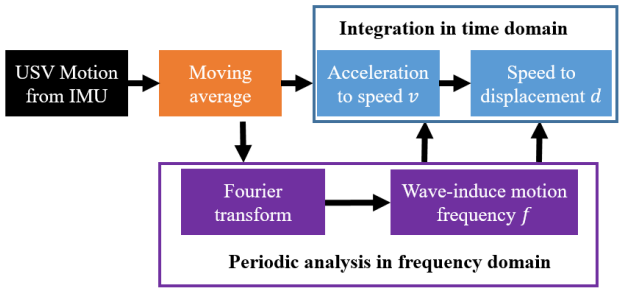

Fig. 5. Time and frequency analysis of the USV motion using the IMU sampling data in water.

A. Time-frequency Analysis of USVs Translational Motion

In this part, the wave-induced USV motion is sampled by an onboard IMU. The USV on the water will be exposed to the wave forces from all directions. Wave models are studied in many researches, for example, [23] and [22] as the most well-known ones. In this paper, the wave is modeled approximately as a combination of sine waves with different amplitudes and frequencies, as said in [22]. Therefore, to analyze the wave-induced translational motion, a comprehensive time-frequency analysis of the IMU data is performed to get the USVs motion.

As shown in Fig.5, raw IMU data is filtered by moving average method to remove the high-frequency noise, and then the filtered IMU data will be used for further analysis. In the frequency domain, the Fourier transformation of IMU data is performed to obtain the respective frequencies of waves. In our onsite experiments in both the harbor and the pool, there is a much more significant frequency with the largest amplitude. This dominant frequency f is treated as the typical wave frequency in our analysis. In the time domain, the wave-induced translational displacement d can be obtained by double integration methods [21] using the IMU data. The integration algorithm consists of double integration from acceleration a to speed v and from v to displacement d.

As said in [21], the double integration of acceleration data will induce an inevitable problem: accumulation errors. This problem will cause inaccuracies of the measurement of the USVs heave motion. In our method, a zero-mean normalization is implemented to eliminate the accumulation errors in all integration operations.

At each time instant t, with the wave period $T = 1/f$ known, the integration step from acceleration a to velocity $v(t)$ is represented by:

$$v(t) = \int_{t-T}^{t} a\, d\tau \tag{6}$$

Then zero-mean normalization based on the zero velocity update (ZVU) principle [21] is implemented by:

$$v_{zm}(t) = v(t) - \frac{\sum_{\tau=t-T}^{t} v(\tau)}{T} \tag{7}$$

where v_{zm} is the normalized velocity data obtained with zero-mean.

The translational displacement d can be obtained by further integration as:

$$d(t) = \int_{t-T}^{t} v_{zm}\, d\tau \tag{8}$$

The displacement range R caused by the wave-induced translational motion in a period can be determined using the following criterion:

$$R(t) = max\{d(\tau)\} - min\{d(\tau)\},\ t - T \le \tau \le t \tag{9}$$

By far, the wave-induced translational motions of the USV have been obtained. The motion will be mainly addressed and analyzed in the experiments. For underwater obstacles avoidance tasks, the vertical heave motion accounts for the most. Considering the USVs safety, operation strategies for different dangerous levels of wave-induced motions are urgently needed.

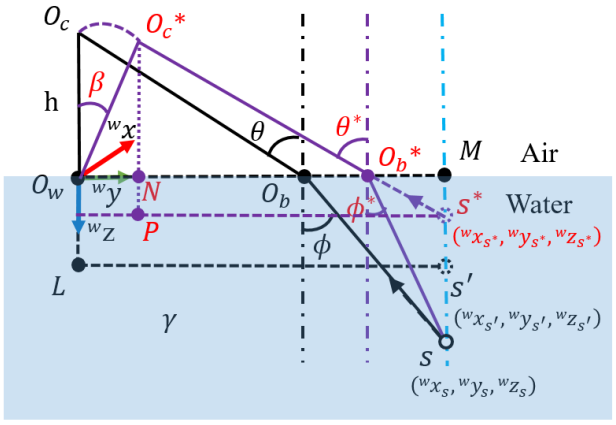

Fig. 6. Illustration of the geometric relations influence by the wave-induced USV rotation. The purple lines indicating the light rays and its symbols are in red. β is the rotation angle. The black lines are the light rays without USV rotation and preserved for comparison.

B. Modeling The Influence for USVs Rotations

The wave-induced translational movement has been modeled in Section.IV-A. For the USV rotations, it will influence the change of light rays incidence angles and the USV draft change in water. Both will induce threats for underwater obstacles collision avoidance and will be addressed in this part.

As shown in Fig.6, the light rays incidence angles with USV rotation are indicated in purple lines. Since camera is installed facing forward on the USV, the pitch rotation will account most for the depth correction. Similar to the modeling in Section.III-B, in the light refraction model with the USVs rotation all the symbols are expressed in red and the definitions are consistent with the addition β as the rotation angle and N, P as the projection on the horizontal lines. Following the same pipeline, the underwater object virtual position S^* can be extracted from the depth map as $(^wx_{s^*}, ^wy_{s^*}, ^wz_{s^*})$. Following the similar geometric relations, the true depth of the obstacles with USV rotation can be obtained as:

$$^wz_s = \frac{^wz_{s*}(\sqrt{(^wx_{s^*})^2 + (^wy_{s^*})^2} - h\sin(\beta))}{\tan\phi(h\cos(\beta) + ^w z_{s*})} \tag{10}$$

For the influence of the USV body draft, the pitch angle $Pitch$ and roll angle $Roll$ will induce the corresponding depth change in water. It can be easily calculated with the USV body width W_{usv} and length L_{usv}.

$$\begin{aligned} \Delta D_{roll} &= \frac{1}{2} L_{usv} * \sin(Pitch) \\ \Delta D_{pitch} &= \frac{1}{2} W_{usv} * \sin(Roll) \end{aligned} \tag{11}$$

The influence of the USV rotations will be addressed and analyzed for USVs underwater obstacles risk assessment in the experiments.

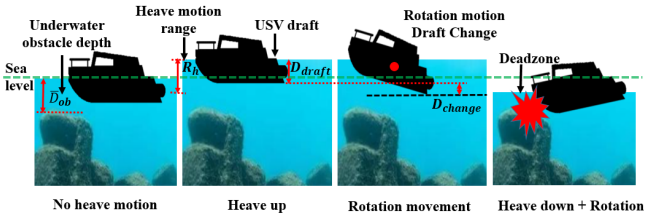

Fig. 7. Scenarios cases when a USV performs tasks with the underwater obstacles and wave-induced USV motion: heave and rotation.

C. Safety Levels Criteria for Wave-induced Motion of USVs

As shown in Fig.7, we define the underwater obstacles rectified depth $\bar{D}_{ob}$, the wave-induced translational heave movement range R_h, the rotation-induced draft change D_{change} and the USV draft D_{draft}, a safe collision avoidance strategy is proposed by defining different safety levels. The wave will induce the USV heave motion: above or below the sea level within R_h with the USV draft $Draft$. Therefore, a safety strategy for the USV exploration tasks with underwater obstacles considering R_h, D_{draft}, D_{change} and $\bar{D}_{ob}$. A three-level safety criterion for underwater obstacles with the

Algorithm 1: Collision avoidance risk assessment for USVs exploration with wave-induced motion

Input: the acceleration of heave motion a
the rectified underwater obstacle depth $\bar{D}_{ob}$
the USV size and draft $L_{usv}, W_{usv}, D_{draft}$
the user-defined safety coefficient S_c

Output: Safety levels: safe, semisafe, deadzone

For each sample time t, N previous data is used.
foreach t **do**
  In frequency domain:
  IMU sample set $A \Leftarrow a[t-N:t]$;
  $\bar{A} \Leftarrow$ Moving average of A;
  $FFT \Leftarrow$ Fast Fourier Transform of $\bar{A}$;
  $f \Leftarrow FFT$ the typical frequency with the largest amplitude in frequency domain;
  In time domain:
  $T \Leftarrow \frac{1}{f}$, IMU $Roll, Pitch$;
  $v \Leftarrow$ Integration of $\bar{A}$;
  $v_{zm} \Leftarrow$ Zero Mean Normalization of v;
  Heave displacement $d \Leftarrow$ Integration of v_{zm};
  Heave range $R_h \Leftarrow max\{d\} - min\{d\}$;
  USV draft change $D_{change} = max\{\Delta D_{roll}, \Delta D_{pitch}\}$;
  if $\bar{D}_{ob} - R_h - D_{change} \leq D_{draft}$ **then**
    Case 1: Safety levels $\Leftarrow deadzone$;
  end
  if $D_{draft} < \bar{D}_{ob} - R_h - D_{change} < S_c * D_{draft}$ **then**
    Case 2: Safety levels $\Leftarrow semisafe$;
  end
  if $\bar{D}_{ob} - R_h - D_{change} \geq S_c * D_{draft}$ **then**
    Case 3: Safety levels $\Leftarrow safe$;
  end
end

user-defined safety coefficient S_c is proposed for the wave-induced motion as in Algorithm.1. We further illustrate them as follows:

- **Case 1:** the safety level is defined as deadzone since the collision between the USV and the obstacle is inevitable, and therefore exploration tasks should be aborted for safety.
- **Case 2:** the safety level is defined as semi-safe zone since the chance of collision still exists due to measurement errors, and therefore USV exploration should be given close attention.
- **Case 3:** the safety level is defined as a safezone since the collision will not happen theoretically. Therefore, it is safe to perform exploration tasks within this area.

V. Experiments and Analysis

In this section, the proposed underwater and surface objects detection and collision avoidance risk assessment is verified and validated with experiments both in a pool and in a sea harbor. First, the platform and the experiment scenarios are presented. Then the experiments analysis of the depth correction and the results of underwater and surface obstacle detection are shown.

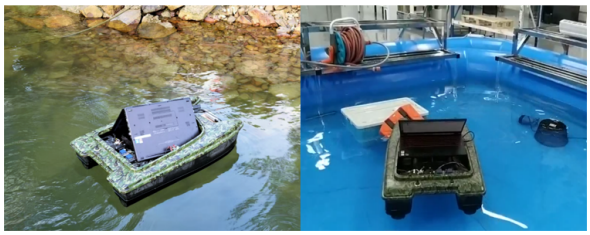

Fig. 8. The USV platform and the working scenarios: nearshore harbor and indoor pool, in the experiments.

A. Experiment Platform and Scenarios

In this part, the USV platform and the working scenarios during an exploration task in the field are shown in Fig.8.

1) Experiment Platform: A small-sized USV is used in our exploration task. As shown in Table.I, the specification of the USV is described in detail. An intel realsense D435i IR stereo camera is installed on the USV, and used to collect both surface and underwater obstacles depth information. An embeded IMU in the D435i measures the USV motion information in disturbance.

TABLE I
The USV platform overview

USV Specificcations					
USV	L_{usv}	W_{usv}	H_{usv}	D_{draft}	**Propeller**
USV-G	0.82m	0.52m	0.23m	6.5cm	Differential Drive Two propeller

2) Experiment Scenarios: As shown in Fig.8, the experiments for our system is verified in two different scenarios: an indoor pool and an open harbor at sea. The indoor pool is with a size of 6.5m×6.5m×0.4m in length, width, and depth. Even the water is shallow in the pool, it is deep enough for the USV since the USV-G draft is only 6.5cm in our experiments. For the harbor at sea, the water is relatively calm and shallow nearshore. In both the two different experiment scenarios, the water is clean and limpid, and this requirement guarantees that the cameras can acquire the visual information of the underwater obstacles.

B. Depth Measurement Correction Experiments

First, to evaluate the proposed depth correction model, as shown in Fig.4, quantitative experiments are conducted in both scenarios. As said in [19], the same evaluation criteria using sample points at different depths is used to evaluate the performance. Seven sets of sample points ranging from 11cm to 38cm are used as a benchmark for evaluation, and raw depth measurement cases are randomly sampled at different time. Then the proposed depth correction algorithm is applied to get the rectified depth of the sample points respectively.

As shown in Fig.9 and Table.II, compared with the benchmark depth, the raw depth of the sample points in different

TABLE II

EXPERIMENTS OF RAW DEPTH AND ITS RECTIFIED DEPTH WITH SAMPLE POINTS AND ITS STATISTICAL INFORMATION

Benchmark Sample Depths /cm	Raw Depth (cm)			Mean (cm)	Std Dev (cm)	Error Ratio	Rectified Depth (cm)			Mean (cm)	Std Dev (cm)	Error Ratio
	Sample 1	Sample 2	Sample 3				Sample 1	Sample 2	Sample 3			
11	1.9	2.4	2	2.1	0.26	80.91%	11.4	12.9	11.8	12.03	0.78	9.36%
14	3.4	3.2	3.2	3.27	0.12	76.64%	14.4	13.6	14.6	14.2	0.53	1.43%
17	6.9	3.7	6.3	5.63	1.7	66.88%	21.4	16.6	17.7	18.57	2.51	9.24%
20	5.3	5.2	4.8	5.1	0.26	74.50%	25.8	22.9	24.1	24.27	1.46	21.35%
21	6.2	3.2	3.3	4.23	1.7	79.86%	20.5	19.6	20.8	20.3	0.62	3.33%
29	5.8	7.6	5.5	6.3	1.14	78.28%	22.8	26.8	18.7	22.77	4.05	21.48%
38	16.3	14.4	10.8	13.83	2.79	63.61%	51.7	44.4	37.5	44.53	7.1	17.18%

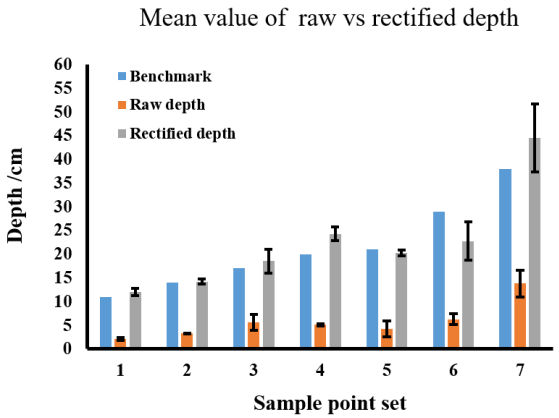

Fig. 9. The mean raw depths vs rectified depths with benchmark data.

depths is far from the benchmark with the error ratio ranging from 63.61% to 80.91%. With the proposed rectified model, the rectified depth achieves much better depth measurement in each depth sample with the error ratio ranging from 1.43% to 21.48%. In the average of all the samples, the error ratio of the raw depth measurement and the rectified depth is 74.38% and 8.94% respectively, and therefore, our proposed method achieves 65.44% significant improvement. In this way, the proposed depth correction algorithm refines the underwater obstacles depth information, and more accurate depth information can be obtained. With the rectified depth, a safer strategy for USVs exploring is proposed in the field.

C. Experiments and Analysis of Wave-induced USV Motions

As said in Section.IV, the wave-induced USV motions include translation and rotation as defined in Fig.1. Their influence will be addressed respectively in this section: translation influence and rotation influence. The statistical information of the USV motion with wave disturbance is analyzed in Table.III.

*1) **Translation Influence**:* As shown in Table.III, by implementing the proposed time-frequency analysis in IV-A, with the sampled IMU data, we conclude our USV translation movements: since the USV will be confined with the water body on the water surface, the heave motion along Z axis will be mainly addressed. The typical wave frequencies for Z axis is f =2-3Hz for both sea and pool experiments. By using this typical wave frequency, the wave-induced USV heave motion range can be concluded as 6.56cm and 0.57cm in pool and sea. For X and Y axis, no water body constraints will stop the USV from movement, therefore, it will move freely on the water surface with the typical wave frequencies $f \approx 0$ Hz. In this situation, the wave-induced USV surge and sway motion range will be the displacement with the integration time. In our experiments, the integration time is 1s, which also means the maximum speed along X and Y axis is about 13.51cm/s and 5.96cm/s in sea and 11.08cm/s and 5.93cm/s in pool. The heave motion will influence the underwater obstacle risk assessment for USVs, and will be discussed in section.V-D.

*2) **Rotation Influence**:* As shown in Table.III, for the wave-induced rotation along the X, Y, Z axes, it will be roll, pitch and yaw angle respectively. For the water body constraints, roll the and pitch angles are relatively small, 2.59 and 2.37 degree change in sea experiments and 8.15 and 6.54 degree change in pool experiments. The maximum angle change is about 10 degrees in all of our experiments. The rotation angle in this wave disturbance is comparable to a big size USV in sea state of 2-3. Therefore, it is representative and reasonable for the USVs. The yaw angle may be large since no constraints are posed the yaw angle on the free water surface. In our sample data, the yaw angle changes from 11.46 to 20 degrees. As described in Section.IV-B, the USV rotation will influence the light incidence angles at the water boundary and the USV draft change in water. This influence will be experimentally quantified with our pool and sea experiments.

The roll and pitch angle will cause USV draft and light rays change, no relation with yaw angle. Therefore, we mainly focus on the wave-induced USV roll and pitch movement. First, we discuss the rotation change influence on the light rays incidence angle as shown in Fig.6. To get maximum incidence angle variation range, we implement the maximum pitch rotation $\pm 5\,\mathrm{deg}$, and calculate the resulted depth motion from raw depth with Equation.(10). As shown in Table.IV, Mean Error in red means the comparison of the wave-induced rotation rectified depths and the rectified depth without rotation influence. Consequently, the rectified depth error ratio with rotation influence is nearly consistent with the original rectified obstacle depth as shown in Table.II, with maximum mean error 0.44cm less than 0.5cm. This is reasonable in our system setup, since our stereo camera is fixed with h=8.5cm and the detection range from the camera ranges from 41.8cm to 82.9cm. In this setup, the rectified depth will suffer from minor influence of the USV rotations. To further elaborate the USV rotations influence in our setup, we validate the rotation angle range β=1-30 degrees with h=8.5cm, ${}^{w}z_{s*}$=15cm and obstacle range 70cm. Since the USV speed is 13.51 cm/s in our experiments and

TABLE III

USV MOTIONS DATA AND ITS RESULTED TRANSLATION OFFSET AND ROTATION ANGLE WITH THE IMU SAMPLE DATA IN EXPERIMENTS

Scenerio		Acceleration (m/s2)					Translation Offset (cm)				Rotation Angle (degree)				
		Max	Min	Mean	Std_Dev	Typical Wave Frequency f	Max	Min	Mean	Std_Dev	Max	Min	Mean	Std_Dev	Range
Sea	X	1.29	0.84	1.07	0.04	0	13.51	13.09	13.26	0.10	1.12	-1.47	0.00	0.55	2.59
	Y	-0.21	-0.77	-0.46	0.06	0	5.96	5.48	5.74	0.11	1.19	-1.18	0.00	0.42	2.37
	Z	-9.44	-9.90	-9.68	0.06	2-3	0.57	0.02	0.16	0.54	14.30	11.34	12.97	0.73	2.96
Pool	X	1.05	0.55	0.73	0.08	0	11.08	8.26	8.79	0.55	3.89	-4.26	0.00	2.06	8.15
	Y	-0.05	-0.77	-0.37	0.14	0	5.93	3.44	4.55	0.43	3.07	-3.47	0.00	1.46	6.54
	Z	-9.01	-10.72	-9.70	0.19	2-3	6.56	0.14	2.22	1.24	20.00	11.46	16.63	1.57	8.55

TABLE IV

RECTIFIED DEPTH WITH THE WAVE-INDUCED USV ROTATION PITCH =$\pm$5 deg IN EXPERIMENTS

Benchmark samples/cm	Rectified Depth with beta=-5			Mean (cm)	Std Dev (cm)	Error Ratio	Mean Error(cm)	Rectified Depth with beta=+5			Mean (cm)	Std Dev (cm)	Error Ratio	Mean Error(cm)
	Case 1	Case 2	Case 3					Case 1	Case 2	Case 3				
11	11.32	12.8	11.72	11.95	0.77	8.64%	-0.08	11.55	13.09	11.96	12.2	0.80	10.91%	0.17
14	14.27	13.47	14.51	14.08	0.54	0.57%	-0.12	14.62	13.81	14.85	14.43	0.55	3.05%	0.23
17	21.17	16.45	17.5	18.37	2.48	8.06%	-0.2	21.7	16.83	17.98	18.84	2.55	10.80%	0.27
20	25.62	22.72	23.95	24.1	1.46	20.50%	-0.17	26.1	23.19	24.4	24.56	1.46	22.82%	0.29
21	20.3	19.48	20.67	20.15	0.61	4.05%	-0.15	20.81	19.83	21.03	20.56	0.64	2.11%	0.26
29	22.62	26.58	18.51	22.57	4.04	22.17%	-0.2	23.12	27.15	18.99	23.09	4.08	20.39%	0.32
38	51.4	44.11	37.22	44.24	7.09	16.42%	-0.29	52.18	44.85	37.89	44.97	7.15	18.35%	0.44

the draft 6.5cm plus the rotation-induced maximum draft 3.57cm in Equation.(11) and heave range is about 6.5cm, the specific parameter are chosen for 5 seconds for altering and safety consideration. The rotation-influenced rectified depth simulation results are shown in Fig.11.

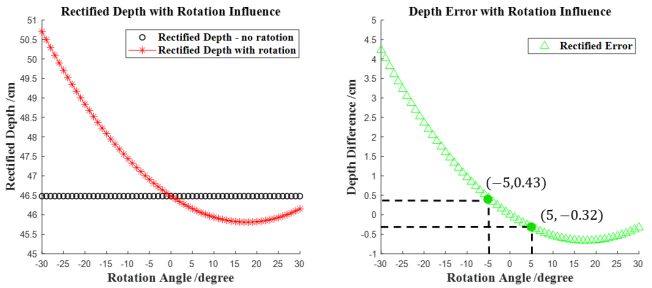

Fig. 10. Simulation of the rectified depth error between the rotation angle along the rotation direction.

From the simulation result, we can see the resultant depth change is minor within 0.5cm. This explains in our setup the wave-induced rotation poses minor influence on the rectified obstacle depth.

For the rotation-induced draft, with the USV L_{usv}=82cm and W_{usv}=52cm from Table.I. With the rotation $\pm$5 deg, the maximum draft changes along X,Y axis are ΔD_{roll}=3.57cm and ΔD_{pitch}=2.27cm. This draft change together with the original draft will be taken for further consideration in the risk assessment for underwater obstacle avoidance risk assessment.

D. Experiments of Underwater and Surface Obstacle Detection and Collision Avoidance Risk Assessment

The proposed surface and underwater obstacle detection methods have been verified for the USV exploration tasks in pool and sea. We have 3 scans performing simultaneously on the extracted depth image: purple scans for surface obstacles; For underwater obstacles, yellow scans and green scans will work with raw depth and rectified depth respectively.

*1) **Underwater and Surface Obstacle Detection**:* As shown in Fig.11, for the surface obstacle stone Obj_7, only the purple scan detects it. Yellow and green scans do not detect it. For the underwater obstacles $Obj\_(3,4,6)$, the yellow and green scans detect them and purple scans do not detect any of them. Obj_2 and Obj_5 are supporting pillars with both underwater and above-water parts. They can be detected by the surface purple scans and the underwater yellow scans. In all experiments, the green scans detection results always lie behind the yellow scans since the green scans work on the depth image with the depth correction. This can be explained as the underwater obstacles are always deeper than the visual depth for the light refraction. Furthermore, to address the proposed depth correction influence during underwater obstacle detection, underwater obstacle Obj_1 in the enlarged view will demonstrate the depth correction influence for obstacle detection. The experiment shows yellow scans detect it as an obstacle and green scans do not. The reason is that the rectified depth information is deeper than our yellow scan detection depth. Therefore, Obj_1 green scans do not treat it as an obstacle. More details will follow in the risk assessment section.

*2) **Collision Avoidance Risk Assessment**:* For the USV safety and the enlargement of exploration areas, different experiments have validated our proposed method. Taking one case study for example, the depth benchmark for Obj_1=21cm, D_{draft}=6.5cm D_{change}=3.57, and the safety coefficient S_c=2 is defined by users in the experiments. Then with the proposed heave modeling and the depth correction algorithm, the calculated heave motion range is R_h=1.38cm, and the mean value of raw and rectified depth is 4.23cm and 20.3cm respectively as shown in Table.II. According to the safety level judgment criteria in Algorithm 1, safety levels are examined:

- For the raw depth information: 4.23-1.38-3.57=-0.72cm<6.5cm, so the Obj_1 is in a deadzone area and thus detected as an obstacle by the yellow scans.
- For the rectified depth information: 20.3-1.38-3.57=15.35cm>13cm=2*6.5cm, so the Obj_1 is in a safe area and therefore not detected by the green scans.

The risk assessment algorithm calculates the underwater

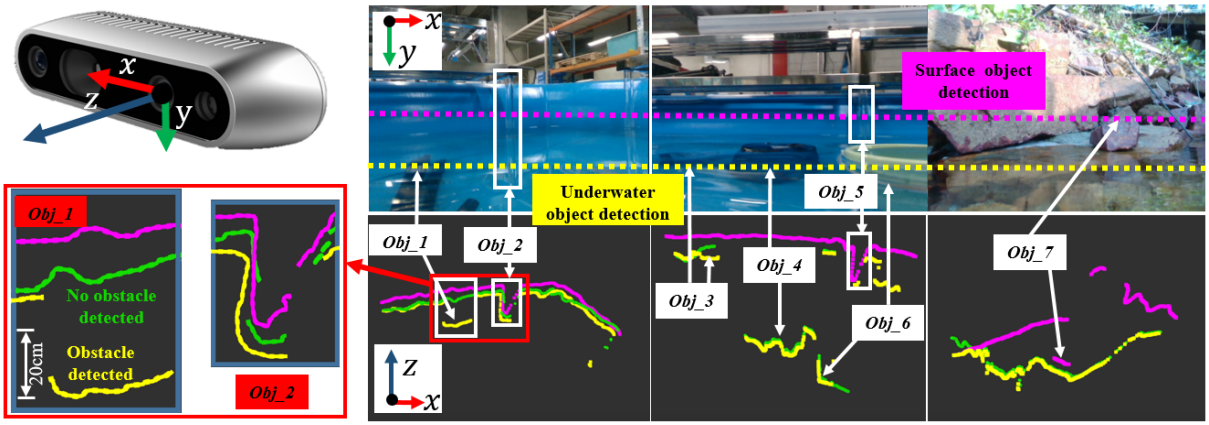

Fig. 11. The surface and underwater object detection in our experiments. Top left, the coordinate of the stereo camera. Down left, the enlarged view of Obj_1 and Obj_2. Top right, the color images. Bottom right: the top down view of scans range of obstacles from the USV. Different colors of scans focus on obstacles in different areas.

obstacles threats online to guarantee the USV safety and further expand the exploration areas in the field.

VI. CONCLUSIONS

In this paper, an underwater and surface obstacle detection system based on the stereo vision and IMU data is originally proposed. This system enables the USV to explore the unknown field in shallow water with collision avoidance of surface and underwater obstacles simultaneously. The proposed system improves the safety and enlarges the USV exploration area. However, other critical issues, like the light variation and water turbidity, will pose challenges and limitations to the accuracy and applicable working scenarios. In the future, a more efficient and robust feature representation with light refraction of the underwater obstacles will be promising for our system so far.

REFERENCES

[1] Z. Liu, Y. Zhang, X. Yu, and C. Yuan, "Unmanned surface vehicles: An overview of developments and challenges," Annu Rev Control, vol. 41, pp. 71-93, 2016.

[2] H. K. Heidarsson and G. S. Sukhatme, "Obstacle detection and avoidance for an autonomous surface vehicle using a profiling sonar," in 2011 IEEE International Conference on Robotics and Automation, 2011: IEEE, pp. 731-736.

[3] B. Bovcon and M. Kristan, "Obstacle detection for usvs by joint stereo-view semantic segmentation," in 2018 IEEE/RSJ International Conference on Intelligent Robots and Systems (IROS), 2018: IEEE, pp. 5807-5812.

[4] T. Huntsberger, H. Aghazarian, A. Howard, and D. C. Trotz, "Stereo vision–based navigation for autonomous surface vessels," J Field Robot, vol. 28, no. 1, pp. 3-18, 2011.

[5] R. Halterman and M. Bruch, "Velodyne HDL-64E lidar for unmanned surface vehicle obstacle detection," in Unmanned Systems Technology XII, 2010, vol. 7692: International Society for Optics and Photonics, p. 76920D.

[6] J. Han, J. Kim, and N.-s. Son, "Persistent automatic tracking of multiple surface vessels by fusing radar and lidar," in OCEANS 2017-Aberdeen, 2017: IEEE, pp. 1-5.

[7] C. Almeida et al., "Radar based collision detection developments on USV ROAZ II," in Oceans 2009-Europe, 2009: Ieee, pp. 1-6.

[8] T. Phanthong, "Real time underwater obstacle avoidance and path re-planning using simulated multi-beam forward looking sonar images for autonomous surface vehicle," Engineering Journal, vol. 19, no. 1, pp. 107-123, 2015.

[9] T. Phanthong, T. Maki, T. Ura, T. Sakamaki, and P. Aiyarak, "Application of A* algorithm for real-time path re-planning of an unmanned surface vehicle avoiding underwater obstacles," Journal of Marine Science and Application, vol. 13, no. 1, pp. 105-116, 2014.

[10] B. Arain, C. McCool, P. Rigby, D. Cagara, and M. Dunbabin, "Improving underwater obstacle detection using semantic image segmentation," in 2019 International Conference on Robotics and Automation (ICRA), 2019: IEEE, pp. 9271-9277.

[11] S. Suresh, E. Westman, and M. Kaess, "Through-water stereo slam with refraction correction for auv localization," IEEE Robotics and Automation Letters, vol. 4, no. 2, pp. 692-699, 2019.

[12] Y. Petillot, I. T. Ruiz, and D. M. Lane, "Underwater vehicle obstacle avoidance and path planning using a multi-beam forward looking sonar," IEEE J Oceanic Eng, vol. 26, no. 2, pp. 240-251, 2001.

[13] A. Chambers et al., "Perception for a river mapping robot," in 2011 IEEE/RSJ International Conference on Intelligent Robots and Systems, 2011: IEEE, pp. 227-234.

[14] J. C. Leedekerken, M. F. Fallon, and J. J. Leonard, "Mapping complex marine environments with autonomous surface craft," in Experimental Robotics, 2014: Springer, pp. 525-539.

[15] W. Wang, B. Gheneti, L. A. Mateos, F. Duarte, C. Ratti, and D. Rus, "Roboat: An Autonomous Surface Vehicle for Urban Waterways," in 2019 IEEE/RSJ International Conference on Intelligent Robots and Systems (IROS), 2019: IEEE, pp. 6340-6347.

[16] C. W. Powers, R. Hanlon, H. Grothe, A. J. Prussin, L. C. Marr, and D. G. Schmale III, "Coordinated sampling of microorganisms over freshwater and saltwater environments using an unmanned surface vehicle (USV) and a small unmanned aircraft system (sUAS)," Front Microbiol, vol. 9, p. 1668, 2018.

[17] A. Agrawal, S. Ramalingam, Y. Taguchi, and V. Chari, "A theory of multi-layer flat refractive geometry," in 2012 IEEE Conference on Computer Vision and Pattern Recognition, 2012: IEEE, pp. 3346-3353.

[18] P. D. Buschinelli, G. Matos, T. Pinto, and A. Albertazzi, "Underwater 3d shape measurement using inverse triangulation through two flat refractive surfaces," in OCEANS 2016 MTS/IEEE Monterey, 2016: IEEE, pp. 1-7.

[19] T. Murase et al., "A photogrammetric correction procedure for light refraction effects at a two-medium boundary," Photogrammetric engineering & remote sensing, vol. 74, no. 9, pp. 1129-1136, 2008.

[20] M. Pedersen, S. Hein Bengtson, R. Gade, N. Madsen, and T. B. Moeslund, "Camera calibration for underwater 3D reconstruction based on ray tracing using Snell's law," in Proceedings of the IEEE Conference on Computer Vision and Pattern Recognition Workshops, 2018, pp. 1410-1417.

[21] M. Benoussaad, B. Sijobert, K. Mombaur, and C. Azevedo Coste, "Robust foot clearance estimation based on the integration of foot-mounted IMU acceleration data," Sensors-Basel, vol. 16, no. 1, p. 12, 2016.

[22] J. Tessendorf, "Simulating Nature: Realistic and Interactive Techniques Simulating Ocean Water," New York: Special Interest Group on Computer Graphics, 2001.

[23] N. Booij, R. C. Ris, and L. H. Holthuijsen, "A third-generation wave model for coastal regions: 1. Model description and validation," Journal of geophysical research: Oceans, vol. 104, no. C4, pp. 7649-7666, 1999.